DOI: 10.26599/FSHW.2026.9251133

Contents lists available at SciOpen

Food Science and Human Wellness

journal homepage: https://www.sciopen.com/journal/2097-0765

China Food Publishing Co.

Time-restricted feeding ameliorates Aβ-induced cognitive impairment in an Alzheimer's disease mouse model through SIRT2-mediated mitochondrial homeostasis

Liyang Rong[a,b], Yating Peng[c], Hao Zhang[a], Guanhua Hu[a], Shasha Wang[a], Yanzi Yu[a], Jiaqun Sun[a], Yi Qiu[a], Bangjiang Fang[d,*], Weirong Li[a,*]

[a] *Science and Technology Innovation Center, Guangzhou University of Chinese Medicine, Guangzhou, China*

[b] *Health Management Centre, Sanya Hospital of Traditional Chinese Medicine (Hainan Hospital, Guangzhou University of Chinese Medicine), Sanya, China*

[c] *School of Basic Medical Sciences, Guangzhou University of Chinese Medicine, Guangzhou, China*

[d] *Department of Emergency, Longhua Hospital, Shanghai University of Traditional Chinese Medicine, Shanghai, China*

ABSTRACT: Alzheimer's disease (AD) is characterized by cognitive decline and impaired brain energy metabolism. Time-restricted feeding (TRF) is a dietary regimen that confines daily food intake to a limited window without caloric reduction, aligning feeding with circadian rhythms and inducing intermittent ketosis. In this study, an 8-hour TRF regimen was compared with a ketogenic diet (KD) in an Aβ-injected AD mouse model to evaluate their effects on cognition and underlying mechanisms. After one month of intervention, TRF significantly improved spatial learning, memory, and recognition in AD mice, with outcomes comparable to or better than KD group. TRF preserved hippocampal neuron morphology, reduced amyloid-β deposition and neuroinflammation, elevated blood and brain β-hydroxybutyrate levels, restored brain ATP levels, and partially rescued mitochondrial respiratory complex activities. Mechanistically, TRF activated the NAD^+-dependent deacetylase SIRT2 in the hippocampus and cortex. SIRT2 activation upregulated PGC-1α and TFAM expression and activated PINK1/Parkin-mediated mitophagy, thereby improving mitochondrial function and energy metabolism. Notably, unlike KD, TRF did not raise blood lipid levels, indicating a superior safety profile. In conclusion, TRF alleviates Aβ-induced cognitive impairment in AD model mice by enhancing SIRT2-mediated mitochondrial homeostasis, supporting TRF as a promising and metabolically balanced intervention for AD.

Keywords: Alzheimer's disease; time-restricted feeding; β-hydroxybutyrate; SIRT2; mitochondrial homeostasis

1. Introduction

Alzheimer's disease (AD) is the leading cause of dementia, characterized by progressive cognitive decline and hallmark neuropathology including extracellular amyloid-β (Aβ) plaques and intracellular tau tangles[1-2]. Beyond these classic lesions, mounting evidence shows that neuronal energy metabolism is severely impaired in AD[3]. In particular, brain glucose uptake and utilization decline early in the disease[4], reflecting defects in the tricarboxylic acid cycle and oxidative phosphorylation. For example, Aβ aggregates

***Corresponding author**
Bangjiang Fang, E-mail address: fangbji@163.com
Weirong Li, E-mail address: liwr@gzucm.edu.cn

Received 10 September 2025
Received in revised from 8 December 2025
Accepted 12 February 2026

disrupt mitochondrial dynamics and biogenesis, triggering excessive mitophagy[5], which depletes ATP and accelerates neuronal damage.

Time-restricted feeding (TRF) is a dietary regimen that confines daily food intake to a limited window (typically ≤10–12 hours) without changing total calories or macronutrient composition[6]. By aligning feeding times with the circadian clock, TRF entrains peripheral metabolic rhythms via regular feeding/fasting cycles[7]. This pattern induces repeated fasting periods during which liver glycogen is depleted, fatty acid oxidation and ketogenesis are increased, raising circulating β-hydroxybutyrate (BHB) levels. In practice, blood BHB often rises to 1–2 mM during overnight fasting[8]. Notably, TRF has been shown in human and animal studies to improve metabolic health even without calorie restriction: it lowers body weight, blood pressure and triglycerides while enhancing glucose regulation[9]. These benefits highlight the synergistic advantages of feeding aligned to circadian biology. In addition to serving as an energy substrate, BHB is a potent signaling metabolite. BHB inhibits class I and IIa histone deacetylases, leading to increased histone acetylation and transcription of protective genes such as FOXO3[10]. It can also covalently modify histones via β-hydroxybutyrylation[11]. Ketone metabolism elevates the NAD^+/NADH ratio, activating NAD^+-dependent deacetylases (sirtuins)[12]. These sirtuins deacetylate transcription factors such as FOXO1/3 and the coactivator PGC-1α to coordinate mitochondrial biogenesis and autophagy[13-14]. BHB further signals through G-protein receptors (e.g. HCAR2/GPR109A) to exert anti-inflammatory effects[15]. Through these combined epigenetic and signaling pathways, nutritional ketosis broadly enhances mitochondrial resilience and cellular stress resistance. SIRT2 is an NAD^+-dependent deacetylase highly expressed in neurons. While predominantly localized in the cytosol, SIRT2 has been found to associate with the mitochondrial inner membrane to directly regulate mitochondrial function[16]. Loss of SIRT2 leads to hyperacetylation of mitochondrial proteins, increased oxidative damage, reduced ATP production, and disrupted autophagy/mitophagy[17], underscoring its role in mitochondrial quality control. Importantly, D-β-hydroxybutyrate has been shown to activate a SIRT2-dependent protective program in neurons: it elevates nuclear FOXO1/3 and PGC-1α levels and stimulates mitochondrial biogenesis, autophagy and mitophagy[18]. These findings suggest that fasting-induced BHB elevations may engage a SIRT2–FOXO–PGC1α axis to restore neuronal mitochondrial function.

Given this potential, dietary strategies that robustly elevate ketone bodies have been explored for neurodegenerative diseases. Both TRF and ketogenic diets (KD) induce ketone production, but their overall metabolic effects differ. KD has been explored as a potential intervention for neurodegenerative diseases[19] and is known to improve several metabolic parameters. Meta-analyses show that KD significantly reduces body weight, HbA1c and triglycerides levels while raising HDL cholesterol[20]. However, its high saturated-fat content can raise total and LDL cholesterol[21], potentially exacerbating cardiovascular risk. In contrast, TRF involves normal dietary patterns and tends to improve dyslipidemia[22]. For example, TRF lowers fasting triglycerides and enhances overall lipid profiles[23], combining the benefits of ketosis with better metabolic health. These differences suggest that TRF might confer unique nutritional advantages over

long-term KD in AD. Critically, no studies to date have directly compared the efficacy of TRF versus KD in AD models. In the present study, we addressed this gap by directly comparing an 8-hour TRF regimen with KD in an Aβ-induced Alzheimer's disease mouse model. We assessed whether TRF rescues cognitive deficits and hippocampal mitochondrial dysfunction through SIRT2-mediated mitochondrial homeostasis and evaluated whether it offers a more favorable lipid and metabolic profile than KD. This work clarifies whether a daily fasting and feeding schedule that induces mild ketosis provides neuroprotective benefits beyond those achieved by sustained ketosis alone.

2. Materials and methods

2.1 Reagents and antibodies

Human $A\beta_{1-42}$ peptide (lot no. P251119-1-SY052487) was procured from GL Biochem (Shanghai, China). RNA extraction reagents (AG RNAex Pro, AG21102), reverse transcription kits (Evo M-MLV RT Premix, AG11728), and quantitative PCR reagents (SYBR Green Pro Taq HS Premix, AG11701) were sourced from Accurate Biology (Hunan, China). The BCA protein assay kit (P0010) and DAPI nuclear stain (C0065) were obtained from Beyotime (Shanghai, China) and Solarbio (Beijing, China), respectively. RIPA lysis buffer (R0010) was purchased from Solarbio (Beijing, China).Primary antibodies included: Rabbit polyclonal anti-APP/Beta Amyloid (25524-1-AP), anti-β-actin (20536-1-AP, lot no. 23021924, housekeeping control), anti-Alpha Tubulin (11224-1-AP, lot no. 56065214, housekeeping control), anti-acetyl-Tubulin (Lys40) (66200-1-lg, lot no. 56025459), anti-SIRT2 (19655-1-AP, lot no. 00059526), anti-FOXO1 (18592-1-AP, lot no. 00394817), anti-FOXO3a (10849-1-AP, lot no. 00157664), anti-MCT2 (20355-1-AP, lot no. 00144827), anti-PGC-1α (66369-1-Ig, lot no. 10027100), and anti-TFAM (22586-1-AP, lot no. 00236521), all supplied by Proteintech (Wuhan, China); anti-IRS-1 (Phospho Ser307, lot no. B4601RC25) (YP0146) supplied by Immunoway (Shanghai, China). Secondary antibodies comprised Rabbit IgG (AS014, Biodragon, Jiangsu, China) and Alexa Fluor™ 488-conjugated Goat anti-Rabbit IgG (H+L) (A-11008, Thermo Fisher Scientific, Shanghai, China). Triglycerides (TG, A110-1-1), total cholesterol (TC, A111-1-1), low-density lipoprotein cholesterol (LDL-C, A113-1-1), and high-density lipoprotein cholesterol (HDL-C, A112-1-1) were purchased from Nanjing Jiancheng Bioengineering Institute (Nanjing, China). Glucose levels were measured using a Glucose (HK) Assay Kit (GAHK20) from Sigma-Aldrich (St. Louis, USA) according to the manufacturer's instructions. NAD^+ and NADH levels were measured using a NAD^+/NADH assay kit (S0175) from Beyotime Biotechnology (Shanghai, China) according to the manufacturer's instructions. The activities of mitochondrial respiratory chain Complexes I (JL49024), Complexes II (JL49033), Complexes III (JL47673), and Complexes IV (JL18155) were determined using assay kits from Jianglai Biotechnology Company (Shanghai, China).

2.2 Animals and treatment

Sixty male C57BL/6J mice (3-month-old, SPF grade) were obtained from Guangdong Medical Laboratory Animal Center (Certificate No. 44007200133990). Synthetic $A\beta_{1-42}$ lyophilized powder (−80°C)

was reconstituted into oligomeric aggregates. Mice were anes**thet**ized with sodium pentobarbital (40 mg/kg, i.p.) and then secured in a stereotaxic frame. Following disinfection from nasal bridge to occiput, scalp incision and blunt dissection exposed the skull. Bilateral hippocampal coordinates (1.8 mm posterior to bregma, ±1.5 mm lateral, 2.0 mm ventral) guided 0.5 mm burr hole drilling. $A\beta_{1-42}$ solution (2 μL/hemisphere, prepared at a concentration of 2 μg/μL) was infused at 0.1–0.2 μL/min via Hamilton syringe, with needle retention for 5 min post-injection. After wound closure, mice recovered in thermoregulated cages (37°C) with ad libitum access to food/water, receiving penicillin G (50,000 IU/kg/day, i.p.) for 3 days. The mice were randomly assigned to four experimental groups (n=15 per group): wild-type (WT) control mice maintained on normal diet, AD model mice receiving normal diet, AD model mice fed a KD serving as the reference intervention group, and AD model mice subjected to time-restricted feeding (TRF). Throughout the 4-week experimental intervention, all animals were housed under controlled environmental conditions with constant temperature (20 ± 2°C), relative humidity (45–55%), and ad libitum access to water. The entire feeding protocol was implemented within the SPF-grade animal facility at Guangzhou University of Chinese Medicine (Sanyuanli Campus, China). The experimental procedures received formal approval from the Institutional Animal Ethics Committee of Guangzhou University of Chinese Medicine (Approval No. 20240414008), with all operations strictly conforming to the ethical 3R principles governing animal research welfare. TRF group underwent an 8:16 h feeding-fasting regimen, with food access permitted exclusively from 08:00 to 16:00 daily. During the 8 h feeding window, mice consumed standard chow ad libitum, while water remained available continuously. The KD group received KD feed (XTKD01, Nika Biotechnology, Hebei, China) composed of 89.91% fat, 10.09% protein, and 0.00% carbohydrate by energy. Both WT control and AD model groups were fed standard diet (1016706714625204224, Ke'ao Xieli Feed Co., Beijing, China) containing 12% fat, 25% protein, and 63% carbohydrate energy equivalents. All diets contained vitamin and mineral supplements. KD, WT, and AD groups maintained ad libitum 24 h food access throughout the study.

2.3 Morris water maze

The Morris water maze was conducted following standard protocols to assess spatial learning and memory. Mice were habituated one week prior to testing. The circular pool (150 cm diameter) was filled with opaque water (21–23 °C) and contained a hidden platform (10 cm diameter) submerged 1 cm below the surface. Acquisition training (Days 2–6) consisted of four trials per day from randomized start positions, with escape latency as the primary measure. On the final day, a probe trial without the platform was performed, and platform-crossing frequency, time spent in the target quadrant, and latency to first target entry were analyzed using the SuperMaze tracking system (Shanghai Xinruan Technology, China).

2.4 Y maze

The Y-maze test was used to evaluate spatial working memory and exploratory behavior. Mice were allowed to freely explore the three-arm apparatus for 5 min following acclimation, and spontaneous alternation behavior was recorded with the VisuTrack system (Shanghai Xinruan Technology, China).

Alternation rate was calculated as the percentage of alternations (entry into an arm that is not one of the previous two arms) out of the total possible alternations, reflecting spatial working memory performance.

2.5 Novel object recognition test

The novel object recognition test was conducted to assess recognition memory based on rodents' preference for novelty. Mice were habituated to the open-field arena for two days before testing. During familiarization, animals explored two identical objects for 5 min, followed 2 h later by a test session in which one object was replaced with a novel one. Exploration times were recorded using the VisuTrack system (Shanghai Xinruan Technology, China). Exploration time was defined as the duration during which the mouse oriented its nose toward the object within a predefined zone surrounding the object (within ~2 cm), including sniffing or direct investigation. Sitting on or passing by the object without active investigation was not counted as exploration. Recognition memory was expressed as a discrimination index calculated as [time exploring the novel object / (time exploring the novel object + time exploring the familiar object) × 100%].

2.6 Nissl stain

Paraffin-embedded brain sections (10 μm) were subjected to Nissl staining with toluidine blue or thionine following standard histological protocols. After deparaffinization, rehydration, staining, and dehydration, sections were mounted and examined under a light microscope (Olympus BX53, Japan), and images were captured using cellSens Standard software.

2.7 H&E stain

Hematoxylin and eosin (H&E) staining was performed on paraffin-embedded hippocampal sections following standard protocols. Stained sections were examined under a light microscope to evaluate neuronal morphology, including cellular architecture, nuclear integrity, and pyknotic changes.

2.8 Immunofluorescence staining

Following transcardial perfusion with PBS and 4% PFA, brains were post-fixed overnight in 4% PFA (4°C), cryoprotected in 15%/30% sucrose, and embedded in O.C.T. compound. Coronal sections (40 μm) were collected using a cryostat (Leica CM1950). After PBS washes, sections underwent blocking in 10% normal goat serum/0.3% Triton X-100, followed by primary antibody incubation in blocking buffer (5% goat serum/0.3% Triton, 24-48 h, 4°C). Secondary antibodies and DAPI nuclear counterstaining were applied in identical blocking conditions. Sections were mounted after final PBS washes and imaged via slide scanning (Olympus VS120).

2.9 Western blot

Brain tissue samples from each group were lysed in RIPA buffer containing protease inhibitors. Protein concentrations were determined using a BCA assay kit. Samples were mixed with loading buffer, denatured at 95°C for 5 min, and separated by SDS-PAGE. Proteins were transferred to PVDF membranes via wet transfer method. Membranes were blocked with 5% non-fat milk in TBST for 2 h at room temperature, then incubated overnight at 4°C with primary antibodies. After washing, HRP-conjugated secondary antibodies were applied

for 1 h at room temperature. Target proteins were visualized using ECL substrate and quantified by densitometry.

2.10 Quantitative real-time PCR

Total RNA was extracted using TRIzol, reverse-transcribed into cDNA with the Evo M-MLV kit. qPCR reactions employed SYBR Green Pro Taq HS Premix on a QuantStudio 5 system. Cycling: 95°C/30s; 40 cycles of 95°C/5s, 60°C/30s. Target genes for qPCR included Pink1, Park2, Map1lc3b, and Sqstm1. Gene expression levels were normalized to β-actin and calculated using the 2^−ΔΔCt method. The primer sequences used are listed in Table 1.

Table 1 The primer sequences

Gene target	Forward sequence	Reverse sequence
Pink1	GAGGAGAAGCAGGCGGAAGG	TGCCAGCATCGAGTGTCCAG
Park2	TTGACACGAGTGGACCTGAGC	ACCTCTGGCTGCTTCTGAATCC
Map1lc3b	GAGCGAGTTGGTCAAGATCATCCG	CATAGATGTCAGCGATGGGTGTGG
Sqstm1	AGGAGGAGACGATGACTGGACAC	TTGGTCTGTAGGAGCCTGGTGAG
β-actin	GTGACGTTGACATCCGTAAAGA	GCCGGACTCATCGTACTCC

2.11 Enzyme-linked immunosorbent assay (ELISA)

Serum concentrations of IL-6 (mI098430), IL-10 (mIC50274-1), IL-17 (ml037866), TNF-α (ml002095), TGF-β (ml057830), BHB (ml415696), and brain tissue levels of BHB and ATP (ml098821) were quantified by ELISA. All procedures followed manufacturer protocols (enzyme-linked Biotechnology, Shanghai, China). Finally,the absorbance was detected using a microplate reader (BioTek Synergy Multifunctional Microwell Plate Testing System, USA). All ELISA kits used in this study were from the same production batch for each analyte.

2.12 Statistical analysis

All quantitative data are presented as mean ± standard deviation (SD). Analyses were performed using GraphPad Prism software (v.9.0.0, GraphPad Software Inc., San Diego, CA, USA). Intergroup differences were assessed by unpaired Student's t-test (two groups) or one-way ANOVA with Tukey's post hoc test (≥3 groups). Statistical significance was defined at $P < 0.05$.

3. Results

3.1 TRF improves cognitive impairment in AD model mice

The experimental timeline is outlined in Fig. 1A. Following successful modeling, AD model mice exhibiting AD histopathological changes and cognitive decline commenced daily 8-hour TRF of standard laboratory chow. Positive control AD model mice received a KD. Both the AD model group mice and the WT control group mice consumed standard laboratory chow ad libitum. Cognitive function testing was performed on all groups one month after the initiation of time-restricted feeding, corresponding to an age of 4 months for all mice (Fig. 1A). Y-maze testing revealed that AD model mice exhibited a significantly lower correct alternation rate compared to WT controls ($P < 0.001$). This cognitive deficit was markedly ameliorated following TRF intervention ($P < 0.001$ vs. untreated AD models; Fig. 1B-C). Notably, TRF achieved

comparable or even better efficacy than the KD-fed positive control group ($P < 0.01$; Fig. 1C). Furthermore, the Morris water maze was used to assess spatial learning and memory. During the training phase, AD model mice exhibited significantly prolonged escape latency compared to WT controls. This deficit was abolished by both TRF and KD interventions ($P < 0.001$; Fig. 1D-E). In the probe trial, AD model mice demonstrated the fewest platform crossings. In contrast, TRF-treated mice showed significantly increased platform crossings and spent more time in the target quadrant compared to untreated AD models ($P < 0.05$; Fig. 1G-H). TRF treatment also significantly shortened escape latency relative to the AD model group ($P < 0.01$; Fig. 1F). To further validate cognitive function, novel object recognition testing was performed. AD model mice showed significantly reduced total movement distance and less time spent exploring the novel object compared to WT controls ($P < 0.05$). In contrast, compared with AD model mice, both TRF- and KD-treated mice showed a significant increase in novel object exploration time ($P < 0.05$; Fig. 1I, J). Collectively, these behavioral results demonstrate that TRF effectively mitigates cognitive decline in AD model mice.

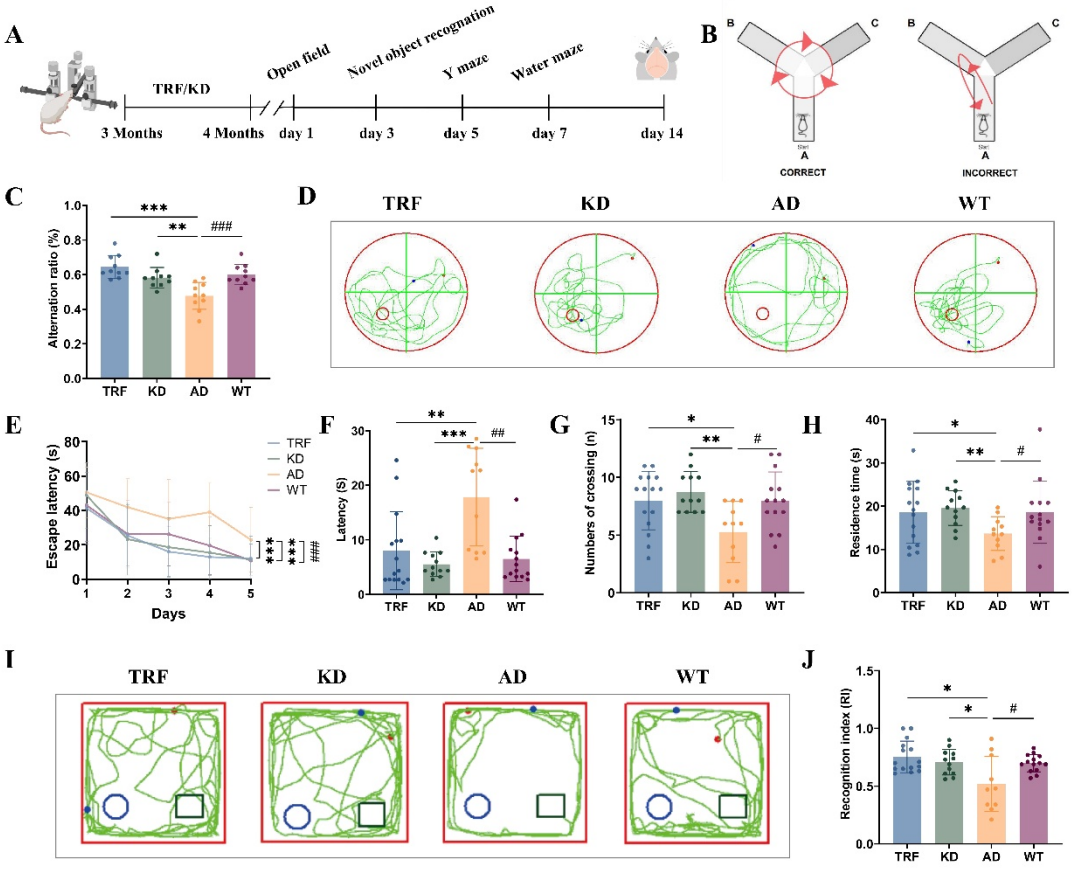

Fig. 1 TRF improved the cognitive function of AD model mice. (A)Schematic diagram of the experimental procedure. (B)Schematic diagram showing the spontaneous alternation behavior correctly exhibited by each group of mice in the Y-maze. (C)The alternating ratios of each group of mice in the Y-maze test ($n = 10$). (D)Prototypical movement traces recorded during Morris water maze behavioral assessment. (E)Escape latency during the 5-day Morris water maze acquisition phase ($n = 10$). (F)The escape latency of each group of mice during the probe trial ($n = 10$). (G)Number of platform crossings per group in the Morris water maze probe trial ($n = 10$). (H)Time spent in target quadrant during probe trial ($n = 10$). (I)Representative exploratory trajectories in the novel object recognition test. The blue dot indicates the starting point of trajectory recording, and the red dot indicates the endpoint of the movement path.(J)Statistical analysis of the cognitive indices of each group of mice in the novel object recognition test ($n = 10$). *n* indicates the number of biological replicates. Data are presented as mean ± SD. $^{*}P < 0.05$, $^{**}P < 0.01$, $^{***}P < 0.001$ vs AD group; $^{\#}P < 0.05$, $^{\#\#}P < 0.01$, $^{\#\#\#}P < 0.001$ vs WT group.

3.2 Effects of TRF on Neuronal Survival

Neuronal apoptosis is a well-established pathological hallmark of AD. To determine whether TRF mitigates neuronal loss in AD model mice, we performed Nissl staining on hippocampal sections. Representative micrographs (Fig. 2A) revealed that WT controls exhibited abundant, uniformly distributed Nissl bodies with large neuronal somata in the DG, CA1, and CA3 subregions. In contrast, the AD model group showed marked neurodegeneration characterized by shrunken somata, reduced/dispersed Nissl bodies, and irregular distribution patterns. Following TRF and KD interventions, both treatments increased Nissl body density and enlarged neuronal somata. Statistical analysis of Nissl-positive cells revealed that TRF administration significantly increased neuronal survival in the DG ($P < 0.01$), CA1 ($P < 0.01$), and CA3 ($P < 0.05$) subfields compared to the AD model group. KD treatment showed increased Nissl-positive cells in the DG ($P < 0.01$) and CA1 ($P < 0.01$), though no statistically significant change was detected in CA3 ($P > 0.05$). These findings suggest that TRF contributes to the preservation of hippocampal neuronal integrity in AD pathology (Fig. 2B-D).

To further evaluate hippocampal neuronal injury, H&E staining was performed on mouse hippocampal tissues. Compared to the WT group, the AD group exhibited increased neuronal translucency, blurred cellular architecture, nuclear pyknosis, and intensified eosinophilia within the hippocampus. However, these aberrant neuronal morphological alterations were ameliorated in the hippocampi of mice subjected to TRF and KD interventions (Fig. 2E). Moreover, quantitative analysis revealed a marked increase in the number of pyknotic nuclei within the CA1, CA3, and DG subregions of the AD group compared to WT controls ($P < 0.001$). Both TRF and KD interventions significantly attenuated Aβ-induced hippocampal neuronal pathology compared to the untreated AD group ($P < 0.05$, $P < 0.01$, $P < 0.001$, respectively; Fig. 2F-H). These findings collectively indicate that time-restricted feeding and ketogenic diet effectively reverse Aβ-induced pathological alterations in hippocampal tissue.

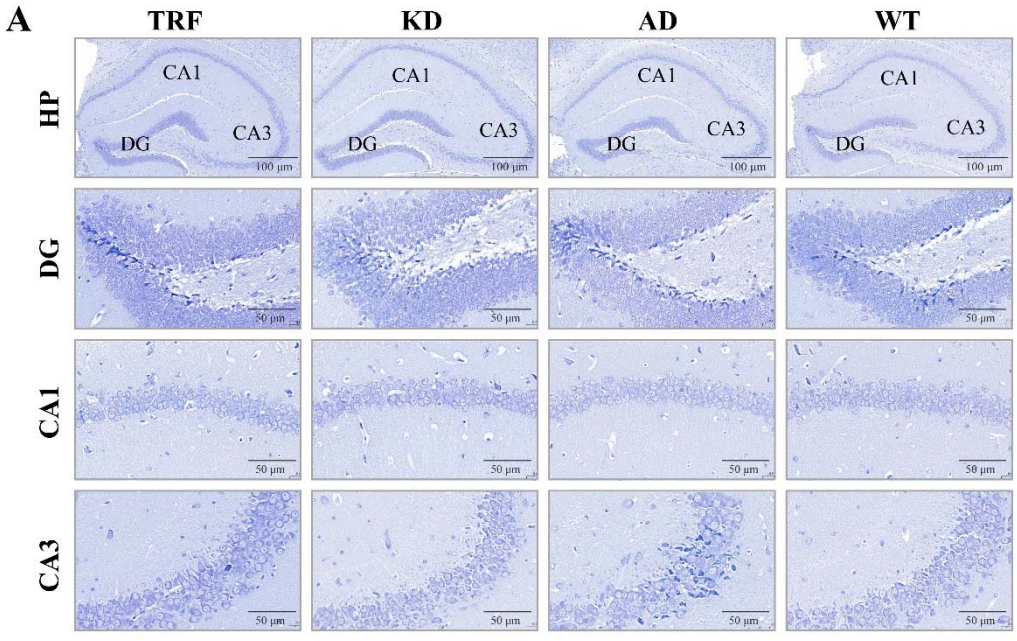

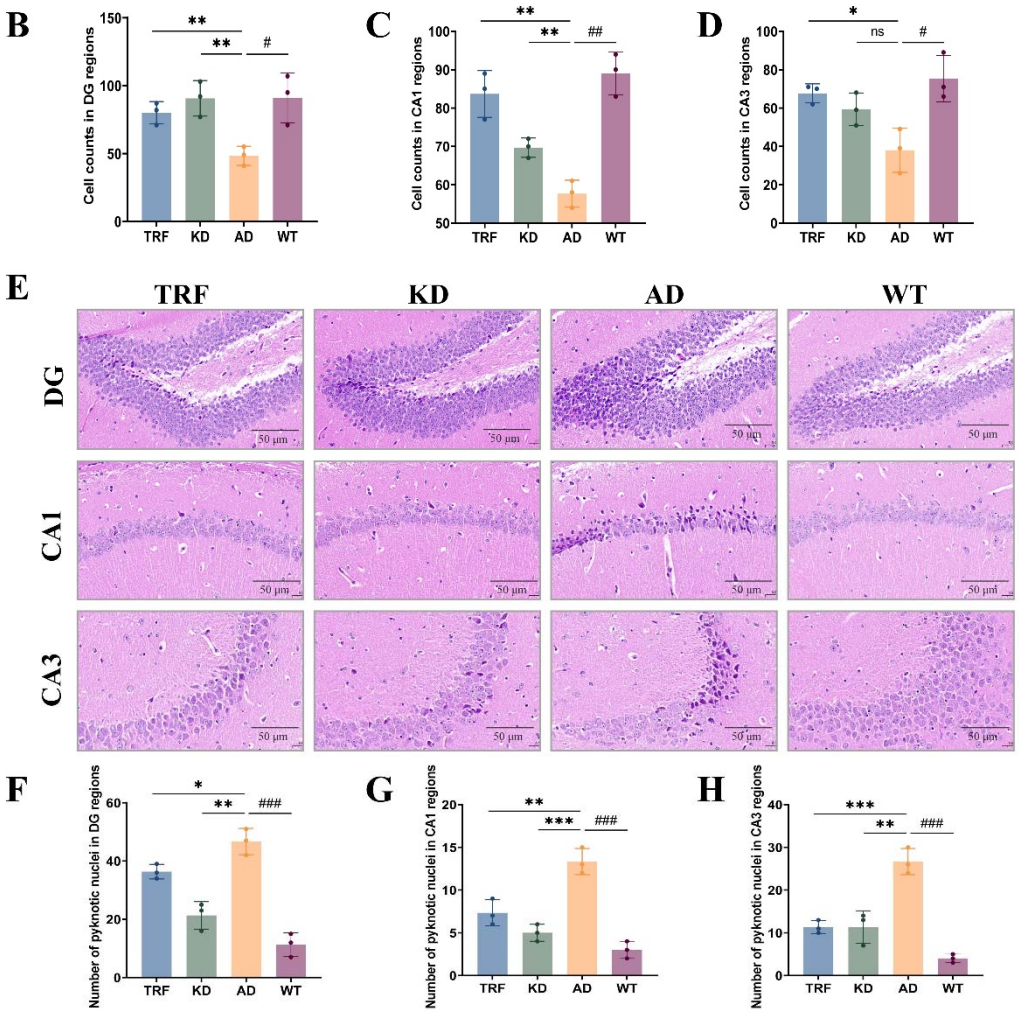

Fig. 2 TRF improves hippocampal neuronal damage in AD model mice. (A)Representative Nissl staining images of the hippocampal DG, CA1, and CA3 subregions in each experimental group. (B)Representative H&E staining images of the hippocampal DG, CA1, and CA3 subregions in each experimental group. (C)Nissl-positive cell counts in the DG subregion by group (n = 3). (D)Nissl-positive cell counts in the CA1 subregion by group (n = 3). (E)Nissl-positive cell counts in the CA3 subregion by group (n = 3). (F)The number of pyknotic nuclei in the DG subregion by group (n = 3). (G)The number of pyknotic nuclei in the CA1 subregion by group (n = 3). (H)The number of pyknotic nuclei in the CA3 subregion by group (n = 3). n indicates the number of biological replicates. Data are presented as mean ± SD. $^{*}P < 0.05$, $^{**}P < 0.01$, $^{***}P < 0.001$ vs AD group; $^{\#}P < 0.05$, $^{\#\#}P < 0.01$, $^{\#\#\#}P < 0.001$ vs WT group; ns, not significant.

3.3 TRF reduces cerebral Aβ deposition and ameliorates neuroinflammation in AD model mice

Accumulation of Aβ triggers neuroinflammation, both constituting integral components of Alzheimer's disease pathogenesis. Given the established correlation between neuronal damage and Aβ deposition coupled with inflammatory responses, we examined cerebral Aβ pathology and quantified hippocampal levels of inflammatory cytokines. Immunofluorescence analysis revealed marked differences in cerebral Aβ deposition across experimental groups (Fig. 3A). WT controls showed no detectable Aβ immunoreactivity, while AD model mice exhibited amyloid plaque formation. Both TRF and KD interventions reduced Aβ deposition, as quantified by Aβ-positive area analysis (Fig. 3B). Statistical comparisons confirmed: WT animals showed significantly less deposition than AD mice ($P < 0.001$), while both TRF and KD groups exhibited reduced amyloid burden versus AD controls ($P < 0.05$ for each comparison). These results indicate that TRF attenuates cerebral amyloid pathology in this AD model.

Neuroinflammation constitutes an integral component of AD pathogenesis. To investigate TRF's potential anti-inflammatory effects, we quantified hippocampal levels of inflammatory cytokines (IL-6, IL-10, IL-17, TNF-α, TGF-β) using ELISA. Compared with WT controls, AD model mice exhibited elevated concentrations of IL-6, IL-17, TNF-α and TGF-β alongside reduced IL-10 in hippocampal tissue, indicating exacerbated neuroinflammatory responses in Alzheimer's pathology. Both TRF and KD interventions reversed these pathological alterations: TRF normalized pro-inflammatory cytokine overproduction (IL-6, IL-17, TNF-α) while restoring anti-inflammatory IL-10 levels, with parallel effects observed in KD-treated animals (Fig. 3C-G). These results demonstrate that TRF effectively attenuates AD-associated neuroinflammation.

3.4 Effects of TRF intervention on hippocampal neuronal structure and ketone transport capacity

Based on the observation that TRF and KD interventions markedly improved neuronal morphology and alleviated pathological damage in AD model mice, we further focused on the hippocampal neurons, which are closely associated with cognitive function, to investigate their functional recovery—particularly energy supply. Given that glucose utilization is impaired in the AD brain, ketone bodies are considered an important alternative energy source, and their uptake depends on monocarboxylate transporter 2 (MCT2). To evaluate the effect of interventions on hippocampal neuronal ketone body uptake capacity, we performed double immunofluorescence staining for NeuN (a marker of mature neurons) and MCT2 in hippocampal tissue (Fig. 3H). The results showed that NeuN fluorescence intensity was significantly higher in the TRF, KD, and WT groups compared with the AD group ($P < 0.05$), indicating improved hippocampal neuronal integrity following intervention (Fig. 3I). MCT2 fluorescence intensity was significantly higher in the TRF and KD groups compared with the AD group ($P < 0.05$), whereas no significant difference was observed between the WT and AD groups. These findings suggest that under normal conditions MCT2 is maintained at a basal level and is not significantly upregulated in the AD model. However, TRF and KD interventions can markedly induce MCT2 expression, potentially enhancing hippocampal neurons' capacity for ketone uptake and utilization (Fig. 3J).

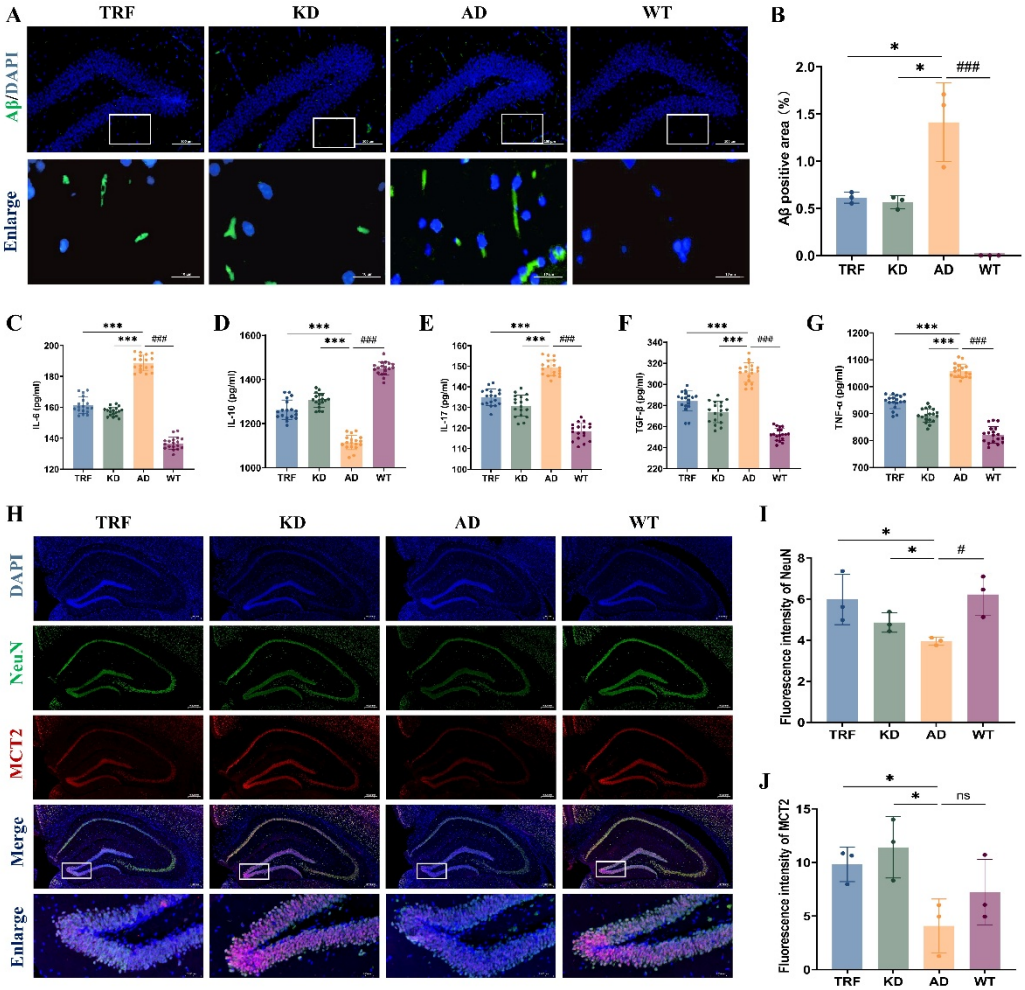

Fig. 3 TRF interventions reduce hippocampal Aβ deposition, attenuate neuroinflammation, and enhance neuronal integrity and ketone transport capacity in AD model mice. (A)Immunofluorescence images showing Aβ deposition in the hippocampus of AD model mice. (B)Statistical analysis of Aβ-positive area (%) in immunofluorescence images (n = 3). (C)Statistical analysis of hippocampal IL-6 concentration (n = 18). (D)Statistical analysis of hippocampal IL-10 concentration (n = 18). (E)Statistical analysis of hippocampal IL-17 concentration (n = 18). (F)Statistical analysis of hippocampal TGF-β concentration (n = 18). (G)Statistical analysis of hippocampal TNF-α (n = 18) concentration. Data are presented as mean ± SD.(H)Double immunofluorescence staining of NeuN (green) and MCT2 (red) in the hippocampus, with DAPI (blue) nuclear counterstaining. Merged images show colocalization of NeuN and MCT2 in neurons. (I)Quantification of NeuN fluorescence intensity (n = 3). (J)Quantification of MCT2 fluorescence intensity (n = 3). n indicates the number of biological replicates. $^{*}P < 0.05$, $^{***}P < 0.001$ vs AD group; $^{\#}P < 0.05$, $^{\#\#\#}P < 0.001$ vs WT group; ns, not significant.

3.5 TRF enhances cerebral energy supply in AD model mice

Building on the observed upregulation of MCT2 in hippocampal neurons following TRF intervention, which suggests enhanced neuronal ketone uptake, we further investigated the effects of TRF on cerebral energy metabolism and mitochondrial function in AD model mice. Compared to WT controls, AD model mice exhibited significantly reduced ATP levels ($P < 0.01$) and decreased NADH concentration ($P < 0.001$) in brain tissue (Fig. 4C-D). Furthermore, activities of mitochondrial complexes I, II, III, and IV were markedly diminished (Fig. 4E-H).

Western blot analysis showed increased inhibitory phosphorylation of IRS-1 at Ser307 in the hippocampus ($P < 0.05$) (Fig. 4A-B), suggesting impaired insulin signaling. Consistently, hippocampal glucose content measured by a hexokinase-based assay was significantly reduced in Aβ-treated mice ($P < 0.01$) (Fig. 4C). TRF intervention significantly increased serum and brain BHB levels ($P < 0.01$), indicating

mild ketosis comparable to that in the KD group (Fig. 4D-E). Concurrently, TRF elevated brain ATP content ($P < 0.01$) and NAD^+/NADH radio in hippocampus ($P < 0.01$) (Fig. 4F-G), and partially restored enzymatic activities of mitochondrial complexes I-IV (Fig. 4H-K).

Transmission electron microscopy (TEM) analysis of hippocampal neuronal ultrastructure revealed notable differences (Fig. 4L). In WT mice, neuronal nuclei (N) exhibited low heterochromatin content, and mitochondria (red arrows) showed intact membranes, clear cristae, and moderate matrix electron density. In contrast, AD mice displayed nuclear pyknosis with increased heterochromatin, swollen mitochondria (blue arrows) with reduced matrix density and disorganized cristae. TRF-treated mice exhibited only mild nuclear heterochromatin increase, with most mitochondria (red arrows) maintaining normal ultrastructure and only a few showing mild swelling and matrix disorganization (blue arrows).

These findings indicate that TRF improves mitochondrial integrity and restores cerebral energy supply, likely mediated by enhanced ketogenesis and increased neuronal ketone uptake.

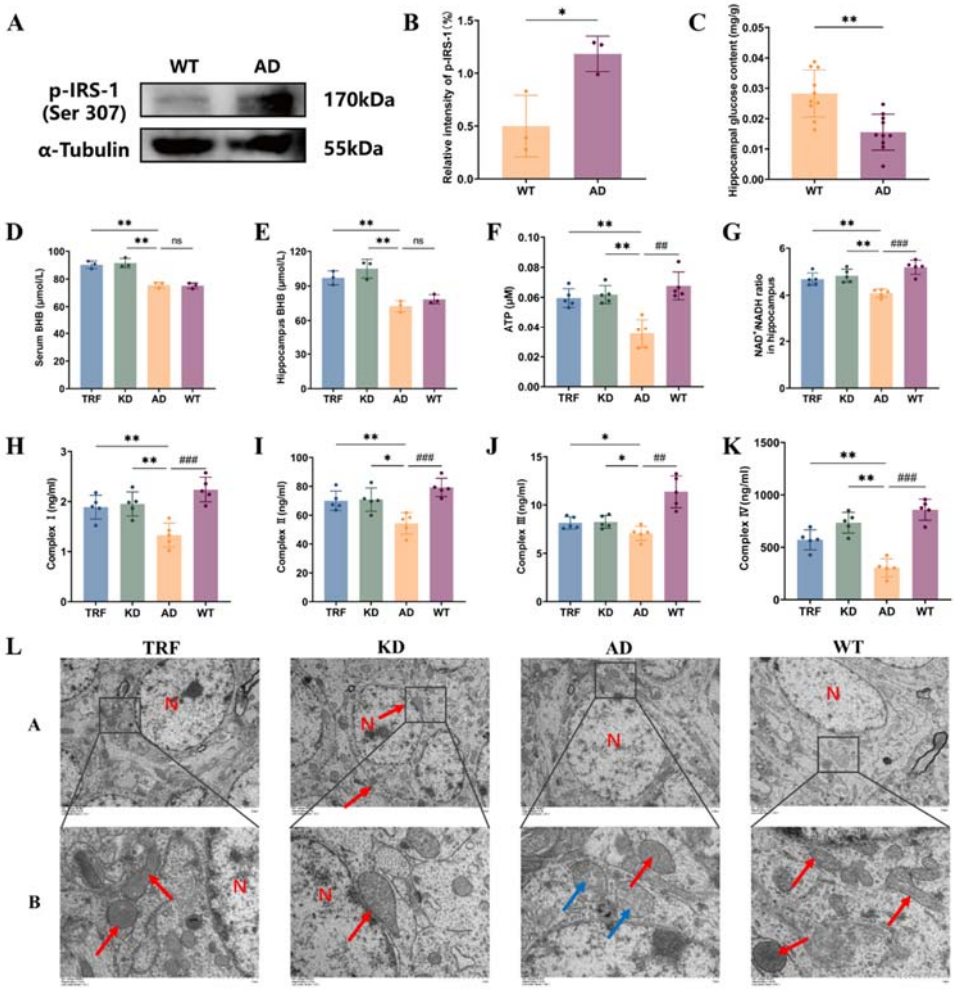

Fig. 4 TRF enhances cerebral energy supply in AD model mice. (A)Western blot bands of p-IRS-1. (B)Quantification of protein expression levels of p-IRS-1 ($n = 3$, technical replicates). (C)Glucose content in hippocampal tissue ($n = 10$). (D)Statistical analysis of serum BHB Levels ($n = 3$). (E)Statistical analysis of hippocampus BHB Levels ($n = 3$). (F)Statistical analysis of ATP levels in brain tissue ($n = 5$). (G)Statistical analysis of NAD^+/NADH radio in brain tissue ($n = 5$）. (H)Statistical analysis of complex I levels in brain tissue ($n = 5$). (I)Statistical analysis of complex II levels in brain tissue ($n = 5$). (J)Statistical analysis of complex III levels in brain tissue ($n = 5$). (K)Statistical analysis of complex IV levels in brain tissue.E-H ($n = 5$). (L)Representative TEM images of hippocampal neuronal ultrastructure. A, Scale bar: 20 μm; B, Scale bar: 10 μm. Red arrows indicate normal mitochondria; blue arrows indicate abnormal mitochondria. N denotes the neuronal nucleus. Data are presented as mean ± SD. $^{*}P < 0.05$, $^{**}P < 0.01$, $^{***}P < 0.001$ vs AD group; $^{\#\#}P < 0.01$, $^{\#\#\#}P < 0.001$ vs WT group; ns, not significant.

3.6 TRF upregulates hippocampal SIRT2 expression to modulate mitochondrial homeostasis

To further determine whether SIRT2 deacetylase function was engaged following TRF and KD interventions, the acetylation status of α-tubulin at Lys40, a well-established substrate of SIRT2, was examined. Western blot analysis showed that acetylated α-tubulin (Lys40) levels were significantly increased in AD mice compared with WT controls, whereas both TRF and KD interventions markedly reduced acetylated α-tubulin levels (Fig. 5A). Quantitative analysis normalized to β-actin demonstrated a significant decrease in acetylated α-tubulin (Lys40) in the TRF and KD groups relative to the AD group (TRF vs AD: $P < 0.01$; KD vs AD: $P < 0.05$), with WT mice also exhibiting lower levels than AD mice (WT vs AD: $P < 0.05$) (Fig. 5B). In contrast, total α-tubulin protein levels normalized to β-actin did not differ significantly among WT, AD, TRF, and KD groups (all $P \geq 0.05$) (Fig. 5C). Consistently, the ratio of acetylated α-tubulin (Lys40) to total α-tubulin was significantly reduced in TRF- and KD-treated mice compared with AD mice (TRF vs AD: $P < 0.01$; KD vs AD: $P < 0.05$), while WT mice again displayed lower ratios relative to AD controls (WT vs AD: $P < 0.05$) (Fig. 5D). Given the significant elevation of cerebral BHB levels following TRF and KD interventions, suggesting ketone bodies as key substrates for improved brain energy metabolism, we focused on examining SIRT2, a known ketone-regulated target, and its downstream pathways in the hippocampus. Western blot analysis revealed significant upregulation of SIRT2 protein expression in TRF and KD groups compared to AD mice (TRF vs AD: $P < 0.05$; KD vs AD: $P < 0.01$) (Fig. 5E-F), indicating that increased BHB may exert protective effects via upregulation of SIRT2 expression. Further investigation showed that the upregulation of SIRT2 expression was accompanied by significant increases in the mitochondrial biogenesis regulators PGC-1α (TRF vs AD: $P < 0.05$; KD vs AD: $P < 0.05$) and TFAM (TRF vs AD: $P < 0.01$; KD vs AD: $P < 0.01$) (Fig. 5E,G-H), suggesting enhanced mitochondrial biogenesis. Meanwhile, nuclear translocation of transcription factors FOXO1 (TRF vs AD: $P < 0.05$; KD vs AD: $P < 0.05$) and FOXO3a (TRF vs AD: $P < 0.01$; KD vs AD: $P < 0.05$) was elevated (Fig. 5I-K), indicating activation of mitophagy-related gene expression. PCR results confirmed that TRF and KD significantly promoted mRNA expression of Pink1 (TRF vs AD: $P < 0.001$; KD vs AD: $P < 0.05$), Park2 (TRF vs AD: $P < 0.05$; KD vs AD: $P < 0.05$), and Map1lc3b (TRF vs AD: $P < 0.05$; KD vs AD: $P < 0.01$), while suppressing transcription of the autophagy adaptor Sqstm1 (TRF vs AD: $P < 0.001$; KD vs AD: $P < 0.01$) (Fig. 5L-O), further supporting enhanced mitophagy activity.Taken together, TRF and KD increase brain BHB levels, activate hippocampal SIRT2, and regulate mitochondrial biogenesis and mitophagy, thereby promoting mitochondrial function restoration and energy metabolism recovery.

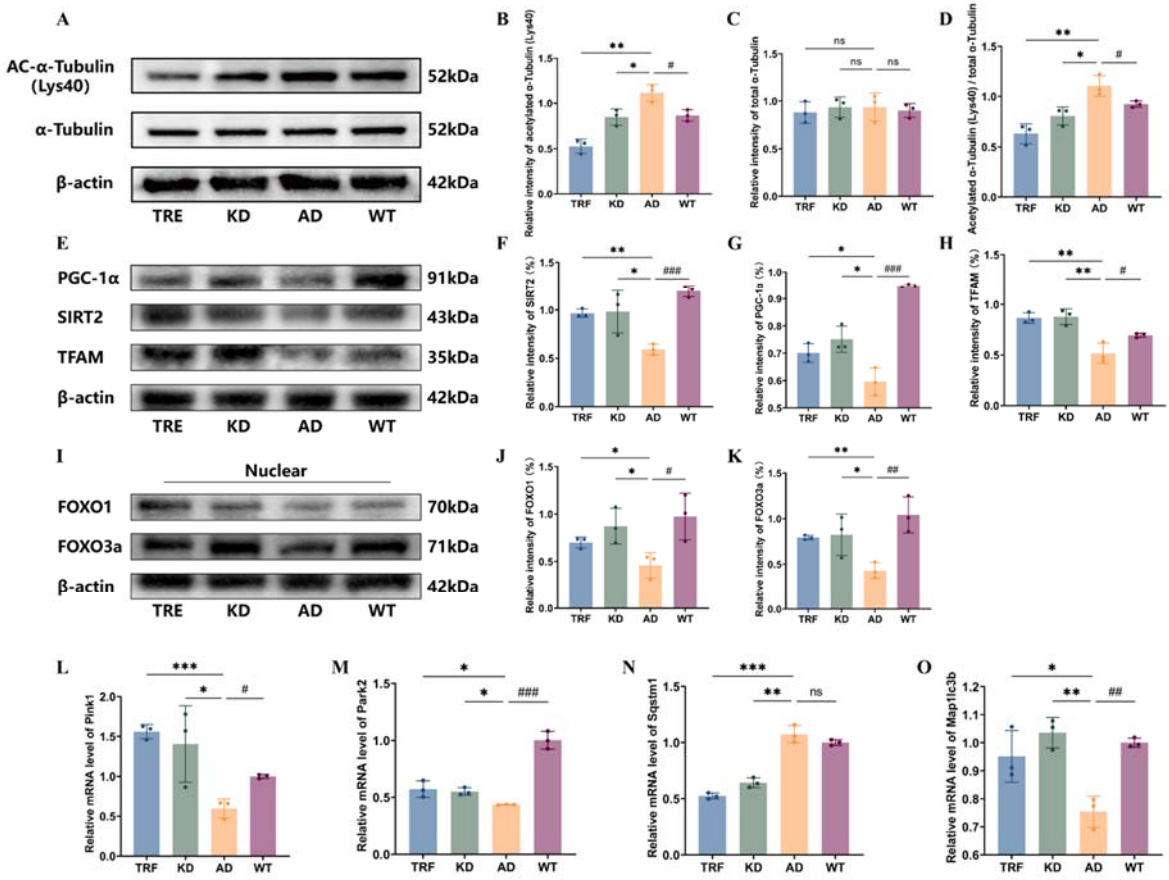

Fig. 5 TRF and KD interventions promote mitochondrial biogenesis and mitophagy in the hippocampus via upregulation of SIRT2 and its downstream signaling. (A)Western blot bands of acetylated-α-Tubulin and total α-Tubulin. (B)Quantification of protein expression levels of acetylated-α-Tubulin ($n = 3$). (C)Quantification of protein expression levels of total α-Tubulin ($n = 3$). (D)Quantification of acetylated α-tubulin (Lys40) normalized to total α-tubulin ($n = 3$). (E)Western blot bands of PGC-1α, SIRT2 and TFAM. (F)Quantification of protein expression levels of SIRT2 ($n = 3$). (G)Quantification of protein expression levels of PGC-1α ($n = 3$). (H)Quantification of protein expression levels of TFAM ($n = 3$). (I) Western blot bands of nuclear FOXO1 and FOXO3a. (J)Quantification of nuclear FOXO1 expression ($n = 3$). (K)Quantification of nuclear FOXO3a expression ($n = 3$). (L-O)mRNA expression levels of mitophagy-related genes Pink1 (L), Park2 (M), Sqstm1 (N), and Map1lc3b (O) detected by PCR ($n = 3$). *n* represents technical replicates. Data are presented as mean ± SD. $^{*}P < 0.05$, $^{**}P < 0.01$, $^{***}P < 0.001$ vs AD group; $^{\#}P < 0.05$, $^{\#\#}P < 0.01$, $^{\#\#\#}P < 0.001$ vs WT group; ns, not significant.

3.7 TRF upregulates cerebral cortex SIRT2 expression to modulate mitochondrial homeostasis

To determine whether SIRT2 deacetylase engagement observed in the hippocampus also occurred in the cerebral cortex, we examined the acetylation status of α-tubulin at Lys40 in cortical tissue. Western blot analysis revealed that acetylated α-tubulin (Lys40) levels were significantly elevated in AD mice compared with WT controls, whereas both TRF and KD interventions markedly reduced acetylated α-tubulin levels in the cortex (Fig. 6A). Quantitative analysis normalized to β-actin showed a significant decrease in acetylated α-tubulin (Lys40) in the TRF and KD groups relative to AD mice (TRF vs AD: $P < 0.05$; KD vs AD: $P < 0.05$), with WT mice also exhibiting lower levels than AD controls (WT vs AD: $P < 0.05$) (Fig. 6B). In contrast, total α-tubulin protein levels normalized to β-actin did not differ significantly among WT, AD, TRF, and KD groups (all $P \geq 0.05$) (Fig. 6C), indicating that the observed changes were not attributable to altered tubulin expression. Consistently, the ratio of acetylated α-tubulin (Lys40) to total α-tubulin was significantly reduced in TRF- and KD-treated mice compared with AD mice (TRF vs AD: $P < 0.001$; KD vs AD: $P < 0.01$), with WT mice again displaying lower ratios relative to AD controls (WT vs AD: $P < 0.01$)

(Fig. 6D). Building on our observations in the hippocampus that TRF and KD interventions elevated cerebral BHB levels and activated SIRT2 and its downstream signaling pathways, we further investigated the applicability of this mechanism in the cerebral cortex. Western blot analysis showed that TRF and KD interventions resulted in statistically significant increases in SIRT2 protein expression compared to AD controls (TRF vs AD: $P < 0.05$; KD vs AD: $P < 0.05$) (Fig. 6E-F), suggesting that BHB may exert effects via SIRT2 activation in the cortex. Meanwhile, key mitochondrial biogenesis regulators PGC-1α (TRF vs AD: $P < 0.01$; KD vs AD: $P < 0.01$) and TFAM (TRF vs AD: $P < 0.001$; KD vs AD: $P < 0.01$) were significantly upregulated (Fig. 6E, G-H), indicating enhanced mitochondrial biogenesis. Nuclear translocation of FOXO1 (TRF vs AD: $P < 0.05$; KD vs AD: $P < 0.05$) and FOXO3a (TRF vs AD: $P < 0.01$; KD vs AD: $P < 0.05$) was also elevated, with significantly higher expression of these proteins in neuronal nuclei compared to AD controls (Fig. 6I, J-K), suggesting potential activation of mitophagy-related gene expression. PCR analyses further demonstrated that TRF and KD significantly increased mRNA expression of mitophagy markers Pink1 (TRF vs AD: $P < 0.001$; KD vs AD: $P < 0.001$), Park2 (TRF vs AD: $P < 0.01$; KD vs AD: $P < 0.01$), and Map1lc3b (TRF vs AD: $P < 0.001$; KD vs AD: $P < 0.001$), while significantly decreasing transcription of Sqstm1 (TRF vs AD: $P < 0.01$; KD vs AD: $P < 0.001$) (Fig. 6L-O), indicating enhanced mitophagy activity.

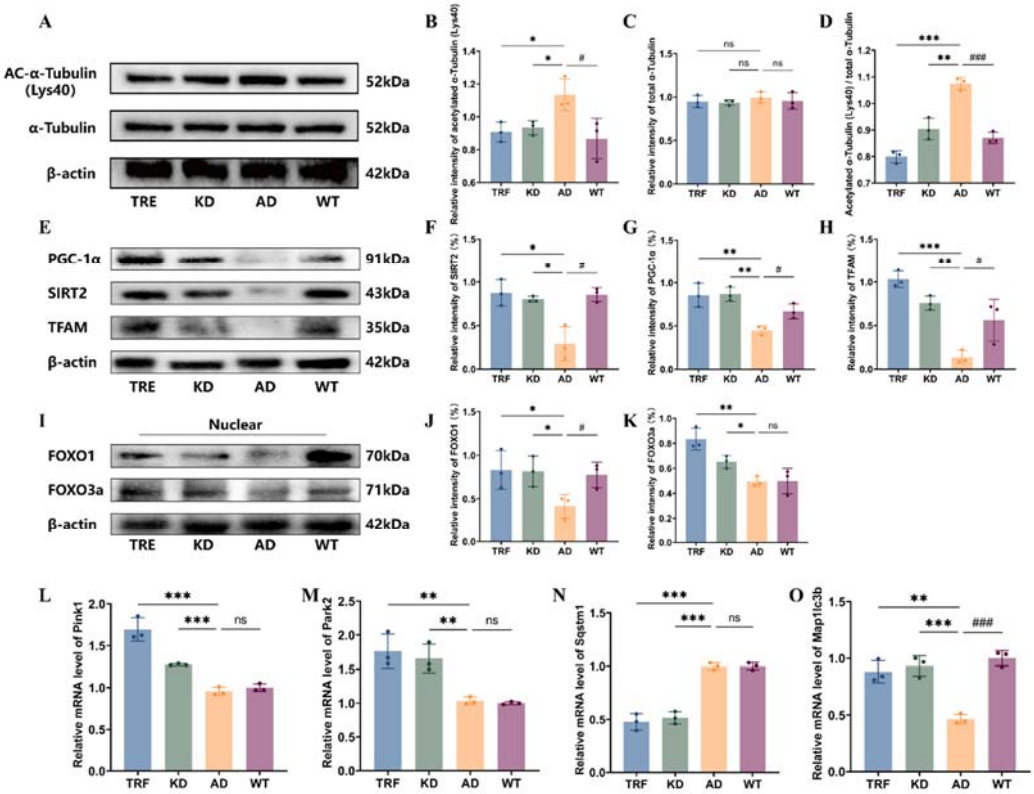

Fig. 6 TRF and KD interventions promote mitochondrial biogenesis and mitophagy in the cortex via upregulation of SIRT2 and its downstream signaling. (A)Western blot bands of acetylated-α-Tubulin and total α-Tubulin. (B)Quantification of protein expression levels of acetylated-α-Tubulin ($n = 3$). (C)Quantification of protein expression levels of total α-Tubulin ($n = 3$). (D)Quantification of acetylated α-tubulin (Lys40) normalized to total α-tubulin ($n = 3$). (E)Western blot bands of PGC-1α, SIRT2 and TFAM. (F)Quantification of protein expression levels of SIRT2 ($n = 3$). (G)Quantification of protein expression levels of PGC-1α ($n = 3$). (H)Quantification of protein expression levels of TFAM ($n = 3$). (I)Western blot bands of nuclear FOXO1 and FOXO3a. (J)Quantification of nuclear FOXO1 expression ($n = 3$). (K)Quantification of nuclear FOXO3a expression ($n = 3$). (L-O)mRNA expression levels of mitophagy-related genes Pink1 (L), Park2 (M), Sqstm1 (N), and Map1lc3b (O) detected by PCR ($n = 3$). n represents technical replicates. Data are presented as mean ± SD. $^{*}P < 0.05$, $^{**}P < 0.01$, $^{***}P < 0.001$ vs AD group; $^{\#}P < 0.05$, $^{\#\#\#}P < 0.001$ vs WT group; ns, not significant.

3.8 Effects of Time-Restricted Feeding on Blood Lipid Profiles

To further compare the effects of TRF and KD on lipid metabolism under comparable therapeutic efficacy, we assessed four serum lipid parameters. The results showed that the KD group exhibited significantly higher TC ($P < 0.001$), LDL-C ($P < 0.01$), and HDL-C ($P < 0.001$) levels compared with the AD group, whereas the TRF group showed no significant differences from the AD group in these parameters ($P > 0.05$). Direct comparison between the two interventions revealed that KD induced significantly higher TC ($P < 0.01$), LDL-C ($P < 0.01$), and HDL-C ($P < 0.001$) levels than TRF. Regarding TG, both TRF and KD groups showed significantly lower levels than the AD group ($P < 0.001$, $P < 0.001$), but KD levels remained higher than those in the TRF group ($P < 0.01$) (Fig. 7A-D). These findings suggest that although both interventions effectively improve cognition and energy metabolism, KD may elevate lipid levels, whereas TRF avoids this adverse effect, thereby offering superior safety.

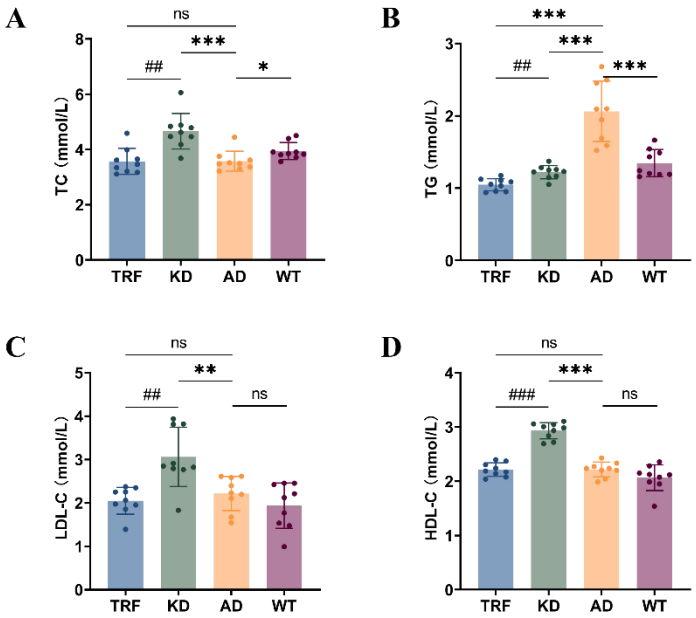

Fig. 7 Effects of TRF on lipid metabolism. (A)Serum total cholesterol (TC) levels ($n = 9$). (B)Serum triglyceride (TG) levels ($n = 9$). (C)Serum low-density lipoprotein cholesterol (LDL-C) levels ($n = 9$). (D)Serum high-density lipoprotein cholesterol (HDL-C) levels ($n = 9$). n represents biological replicates. Data are presented as mean ± SD. $^{*}P < 0.05$, $^{**}P < 0.01$, $^{***}P < 0.001$ vs AD group; $^{\#\#}P < 0.01$, $^{\#\#\#}P < 0.001$, TRF vs KD group; ns, not significant.

4. Discussion

In our Aβ-induced mouse model, a TRF regimen markedly improved learning and memory compared to controls, echoing reports that TRF reduces amyloid plaque burden and restores cognition in AD mice[9, 24]. TRF's benefits are often attributed to aligning feeding with circadian rhythms. However, because our mice are nocturnal and were fed during the light phase when they are normally inactive, the benefits of TRF likely stemmed from the fasting cycle itself rather than circadian alignment. In our study, TRF's daily fasting period raised blood β-hydroxybutyrate and lowered glucose, indicating a shift to ketosis. These changes may engage energy-sensing pathways in which low glucose and high ketones activate AMPK and suppress mTOR[25], thereby stimulating autophagy including mitophagy. We did not measure AMPK or mTOR directly, but increased mitophagy markers in TRF mice suggest enhanced autophagic "cleanup" of misfolded proteins and damaged organelles, reducing their toxic and inflammatory impact. Additionally, β-hydroxybutyrate can

upregulate brain-derived neurotrophic factor (BDNF)[26], which promotes mitochondrial biogenesis and synaptic plasticity; although we did not measure BDNF, this mechanism may also contribute to TRF's benefits. Thus, the daily metabolic and neurotrophic stimulation by TRF may preserve mitochondrial health and support synaptic function in the AD brain.

TRF increased hippocampal expression of genes for mitochondrial quality control. Mitophagy regulators Pink1 and Park2 were significantly upregulated, and mitochondrial biogenesis factors PGC-1α and TFAM were elevated. This aligns with reports that intermittent fasting enhances mitochondrial biogenesis and mitophagy in neural tissue[27]. In contrast, AD mice with ad libitum feeding accumulated more dysfunctional mitochondria, reflecting the impaired mitochondrial dynamics seen in previous studies. TRF appears to rebalance mitochondrial dynamics, as fasting can increase mitochondrial mass and optimize the fusion-fission equilibrium while also inducing mitophagy to clear damaged mitochondria[28-29]. By clearing defective mitochondria and generating new ones, TRF helps sustain cellular energy production and prevent the energy deficits typical of AD neurons. These mitochondrial improvements likely underlie TRF's superior cognitive benefits.

An intriguing finding was that TRF activated the SIRT2 pathway in the hippocampus. SIRT2 is an NAD^+-dependent deacetylase predominantly in the cytosol, and although we did not directly measure NAD^+ or the NAD^+/NADH ratio, fasting-driven changes in these metabolites may contribute to its activation[30]. Activated SIRT2 deacetylates metabolic enzymes, shifting cellular metabolism toward stress resistance. For example, SIRT2 can promote the pentose phosphate pathway by deacetylating G6PD, thereby boosting NADPH production and antioxidant capacity[31]. Moreover, SIRT2 interacts with circadian clock components and autophagy regulators[32-33]. Thus, SIRT2 could link the feeding-fasting cycle to metabolic reprogramming, coordinating energy homeostasis with circadian signals. However, SIRT2's role in AD is complex. Excessive SIRT2 activity impaired autophagy and cognition in one study, whereas SIRT2 inhibition improved memory and autophagy in aged mice[34]. This suggests TRF's benefits depend on fine-tuning SIRT2: moderate activation may bolster neuronal resilience, but overactivation might hinder protein clearance. Overall, our findings indicate that TRF engages sirtuin pathways to shift neurons into a protective metabolic state. Further research is needed to clarify SIRT2's contribution to TRF's effects. For instance, it would be useful to measure brain NAD^+ levels and SIRT2 activity, and to test whether blocking SIRT2 diminishes TRF's benefits.

In contrast, the KD yielded some overlapping metabolic effects but produced weaker outcomes than TRF. Like TRF, KD elevates ketones and can improve mitochondrial function and reduce oxidative stress in AD models[35]. For instance, Auwera et al. reported that a high-fat KD reduced brain Aβ levels by about 25% and enhanced mitochondrial respiration in APP-transgenic mice[36]. However, the cognitive benefits of KD have been inconsistent, and despite metabolic improvements many studies report only modest or no memory gains[37]. In our experiment, the KD group likewise exhibited elevated ketones and a slight reduction in brain Aβ, but only minimal improvement in cognitive performance compared to TRF. This disparity likely reflects

fundamental differences between the approaches. KD induces sustained ketosis without fasting intervals or circadian re-entrainment, whereas TRF imposes a daily fasting-feeding cycle that triggers additional protective pathways. The metabolic rhythm under TRF may engage broader mechanisms such as circadian gene expression changes, pulsatile autophagy, and synaptic plasticity adaptations beyond merely switching energy substrates.

Importantly, the safety profiles of TRF and KD differ markedly. KD is difficult to sustain and can cause adverse effects. Studies have documented acute KD side effects ("keto flu"), including gastrointestinal symptoms (nausea, diarrhea, constipation, abdominal pain) along with headache and fatigue[38]. Over longer periods, KD can lead to vitamin and mineral deficiencies, hyperlipidemia, kidney stones, and hyperuricemia[39]. In our study, KD mice developed higher blood cholesterol, whereas TRF mice did not, underscoring TRF's safer metabolic profile. Importantly, systemic lipid metabolism is not only a safety concern but also a mechanistic factor shaping brain mitochondrial homeostasis. Chronic lipid overload generates a pro-oxidative metabolic environment characterized by elevated circulating lipids and lipid peroxidation products, which can impair mitochondrial respiration, amplify reactive oxygen species production, and disrupt mitochondrial quality control[40]. Moreover, excessive peripheral lipids have been shown to compromise blood–brain barrier integrity and promote microglial activation, thereby exacerbating neuroinflammation and mitochondrial stress within the brain[41]. In this context, the elevated blood cholesterol observed in KD-fed mice may impose an additional metabolic burden on neuronal mitochondria, potentially offsetting the benefits of sustained ketosis. By contrast, TRF induces transient and rhythmically organized lipid mobilization without chronic lipid excess, creating a metabolically restrained environment that more effectively supports mitochondrial renewal, redox balance, and neuronal resilience. Moreover, TRF only alters meal timing and carries far fewer risks. Nonetheless, excessively long fasting windows could result in undernutrition, especially in frail or advanced AD patients[42]. For relatively healthy or early-stage AD individuals, a 10~12-hour daytime feeding window can improve metabolic health with minimal side effects[43]. More vulnerable patients may require a more flexible TRF schedule to ensure adequate nutrition. Overall, while both TRF and KD aim to mitigate brain hypometabolism, TRF offers a more holistic and potentially safer approach by harnessing innate circadian and autophagic mechanisms, whereas KD demands strict macronutrient changes and carries a higher risk of metabolic complications.

Our findings support the concept that TRF could be a practical dietary strategy to promote brain health in AD. Although in our study TRF was implemented during the light phase when mice are normally inactive, the consistent fasting-feeding cycle itself may underlie the observed benefits. Whether alignment with the active phase is necessary requires further investigation[44]. In contrast to KD, which demands a drastic macronutrient overhaul, TRF simply shifts the timing of meals. Early human data, though limited, are encouraging: an observational study found that older adults who limited their eating to about 10 hours per day had significantly better cognitive scores than those with longer eating windows[45]. This aligns with the emerging field of "chrono-nutrition", which posits that concentrating food intake during the day may preserve neuronal

function. TRF is accessible and low-cost, and it could complement pharmacological therapies by improving metabolic resilience.

Several limitations of the present study should be acknowledged. First, although the intracranial Aβ injection model is widely used to induce AD-like cognitive impairment and amyloid-related pathology, it does not fully recapitulate the complexity of Alzheimer's disease, as it lacks key features such as tau neurofibrillary tangles, chronic neuroinflammation, and progressive neuronal degeneration. In addition, the absence of a sham-operated control group prevents complete exclusion of potential effects attributable to the surgical procedure itself. Nevertheless, prior studies using similar paradigms indicate that sham or vehicle injections alone do not cause sustained behavioral or mitochondrial alterations, supporting that the observed changes are primarily driven by Aβ exposure. Second, a WT+TRF group was not included; therefore, the effects of TRF on healthy mice were not directly assessed. Our experimental design focused on evaluating the therapeutic efficacy of TRF under Aβ-induced pathological conditions, and future studies incorporating WT animals will be necessary to clarify its physiological impact. Third, the relatively short observation period precludes assessment of the long-term safety and sustainability of TRF. In addition, as mice are nocturnal and food restriction was applied during the light phase, the optimal feeding window in humans may differ. Finally, although mechanistic evidence was strengthened by assessing the NAD^+/NADH redox status and functional readouts of SIRT2 deacetylase engagement, further causal validation, such as pharmacological or genetic inhibition of SIRT2, will be valuable. Despite these limitations, our findings support TRF as a metabolically balanced intervention that improves cerebral energy homeostasis in an AD-like context.

5. Conclusion

This study establishes that TRF significantly ameliorates cognitive impairment and hippocampal neuronal damage in Aβ-induced AD model mice. The neuroprotection is mediated by a fasting-induced increase in circulating BHB, which activates the SIRT2 signaling pathway in neurons. SIRT2 activation orchestrates mitochondrial homeostasis through dual mechanisms: it enhances mitochondrial biogenesis by upregulating the transcriptional coactivator PGC-1α and mitochondrial transcription factor TFAM, while concurrently promoting mitophagy via nuclear translocation of FOXO1/FOXO3a and subsequent activation of the PINK1/Parkin pathway (Fig. 8). These coordinated actions restore cerebral ATP production and mitochondrial complex activities, thereby resolving neuronal energy deficits. Critically, TRF achieves cognitive benefits comparable to KD without elevating total cholesterol or low-density lipoprotein levels, demonstrating its superior safety profile, potentially linked to the fasting-feeding cycle rather than circadian alignment itself. These findings position TRF as a translatable and metabolically balanced dietary intervention against AD pathogenesis.

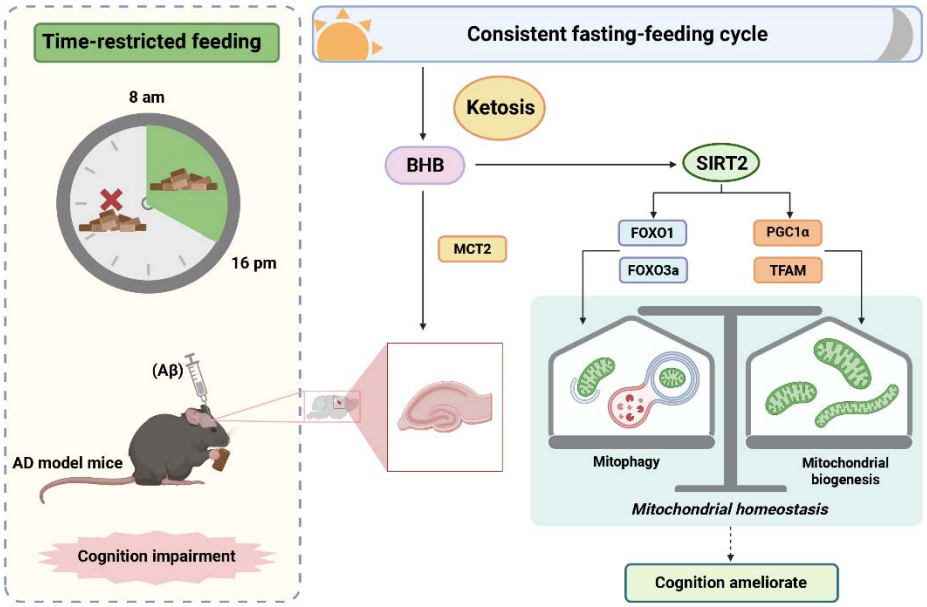

Fig. 8 Schematic representation of the experimental mechanism. An 8-hour time-restricted feeding regimen induces mild ketosis and elevates BHB, which activates SIRT2 to drive FOXO-mediated mitophagy and PGC-1α/TFAM-mediated mitochondrial biogenesis, thereby restoring mitochondrial homeostasis and alleviating Aβ-induced neuronal and cognitive impairment.

Funding sources

This work was supported by the National Natural Science Foundation of China (82074505, 82374547); Guangdong Basic and Applied Basic Research Foundation (2023A1515011835); and the Traditional Chinese medicine inheritance innovation development research project of Zhongshan (2024B3024).

Declaration of competing interest

The authors declare that they have no known competing financial interests or personal relationships that could have appeared to influence the work reported in this paper.

References

Xiaopeng, Z., Jing, Y., Xia, L., et al. Global Burden of Alzheimer's disease and other dementias in adults aged 65 years and older, 1991-2021: population-based study. Frontiers in public health 13 (2025) 1585711. https://doi.org/10.3389/fpubh.2025.1585711.

Moreira, P., Matos, P., Figueirinha, A., et al. Forest Biomass as a Promising Source of Bioactive Essential Oil and Phenolic Compounds for Alzheimer's Disease Therapy. International journal of molecular sciences 23 (2022) 8812. https://doi.org/10.3390/ijms23158812.

Wang, W., Zhao, F., Ma, X., et al. Mitochondria dysfunction in the pathogenesis of Alzheimer's disease: recent advances. Molecular neurodegeneration 15 (2020) 30. https://doi.org/10.1186/s13024-020-00376-6.

Harris, W. J., Asselin, M. C., Hinz, R., et al. In vivo methods for imaging blood-brain barrier function and dysfunction. European journal of nuclear medicine and molecular imaging 50 (2023), 1051–1083. https://doi.org/10.1007/s00259-022-05997-1.

de la Cueva, M., Antequera, D., Ordoñez-Gutierrez, L., et al. Amyloid-β impairs mitochondrial dynamics and autophagy in Alzheimer's disease experimental models. Scientific reports 12(2022) 10092. https://doi.org/10.1038/s41598-022-13683-3.

Halder, S. K., Melkani, G. C. The Interplay of Genetic Predisposition, Circadian Misalignment, and Metabolic Regulation in Obesity. Current obesity reports 14(2025) 21. https://doi.org/10.1007/s13679-025-00613-3.

Longo, V. D., Panda, S. Fasting, Circadian Rhythms, and Time-Restricted Feeding in Healthy Lifespan. Cell metabolism 23(2016) 1048–1059. https://doi.org/10.1016/j.cmet.2016.06.001.

Jang, Y., Kim, Y. S., Kim, S. R., et al. Intermittent Fasting Protects Against the Progression from Acute Kidney Injury to Chronic Kidney Disease. Antioxidants (Basel, Switzerland) 14(2025) 119. https://doi.org/10.3390/antiox14010119.

Whittaker, D. S., Akhmetova, L., Carlin, D., et al. Circadian modulation by time-restricted feeding rescues brain pathology and improves memory in mouse models of Alzheimer's disease. Cell metabolism 35(2023) 1704–1721 e6. https://doi.org/10.1016/j.cmet.2023.07.014.

Newman, J. C., Verdin, E. β-hydroxybutyrate: much more than a metabolite. Diabetes research and clinical practice 106(2014) 173–181. https://doi.org/10.1016/j.diabres.2014.08.009.

Xie, Z., Zhang, D., Chung, D., et al. Metabolic Regulation of Gene Expression by Histone Lysine β-Hydroxybutyrylation. Molecular cell 62(2016) 194–206. https://doi.org/10.1016/j.molcel.2016.03.036.

Hsu, F. Y., Liou, J. Y., Tang, F. Y., et al. Ketogenic Diet Consumption Inhibited Mitochondrial One-Carbon Metabolism. International journal of molecular sciences 23(2022) 3650. https://doi.org/10.3390/ijms23073650.

Zhang, T., Wang, L., Duan, X., et al. Sirtuins mediate mitochondrial quality control mechanisms: a novel therapeutic target for osteoporosis. Frontiers in endocrinology 14(2024) 1281213. https://doi.org/10.3389/fendo.2023.1281213.

Lagunas-Rangel F. A. Sirtuins in mitophagy: key gatekeepers of mitochondrial quality. Molecular and cellular biochemistry (2025). 10.1007/s11010-025-05358-0. Advance online publication. https://doi.org/10.1007/s11010-025-05358-0.

Graff, E. C., Fang, H., Wanders, D., et al. Anti-inflammatory effects of the hydroxycarboxylic acid receptor 2. Metabolism: clinical and experimental 65(2016) 102–113. https://doi.org/10.1016/j.metabol.2015.10.001.

Liu, G., Park, S. H., Imbesi, M., et al. Loss of NAD-Dependent Protein Deacetylase Sirtuin-2 Alters Mitochondrial Protein Acetylation and Dysregulates Mitophagy. Antioxidants & redox signaling 26(2017) 849–863. https://doi.org/10.1089/ars.2016.6662.

Lee I. H. Mechanisms and disease implications of sirtuin-mediated autophagic regulation. Experimental & molecular medicine 51 (2019) 1–11. https://doi.org/10.1038/s12276-019-0302-7.

Gómora-García, J. C., Montiel, T., Hüttenrauch, M., et al. Effect of the Ketone Body, D-β-Hydroxybutyrate, on Sirtuin2-Mediated Regulation of Mitochondrial Quality Control and the Autophagy-Lysosomal Pathway. Cells 12(2023) 486. https://doi.org/10.3390/cells12030486.

Hersant, H., Grossberg, G. The Ketogenic Diet and Alzheimer's Disease. The journal of nutrition, health & aging 26(2022) 606–614. https://doi.org/10.1007/s12603-022-1807-7.

Tao, Y., Leng, S. X., Zhang, H. Ketogenic Diet: An Effective Treatment Approach for Neurodegenerative Diseases. Current neuropharmacology 20(2022) 2303–2319. https://doi.org/10.2174/1570159X20666220830102628.

Bueno, N. B., de Melo, I. S., de Oliveira, S. L., et al. Very-low-carbohydrate ketogenic diet v. low-fat diet for long-term weight loss: a meta-analysis of randomised controlled trials. The British journal of nutrition, 110(7)(2013), 1178–1187. https://doi.org/10.1017/S0007114513000548.

Patikorn, C., Roubal, K., Veettil, S. K., et al. Intermittent Fasting and Obesity-Related Health Outcomes: An Umbrella Review of Meta-analyses of Randomized Clinical Trials. JAMA network open 4(2021) e2139558. https://doi.org/10.1001/jamanetworkopen.2021.39558.

Aouichat, S., Chayah, M., Bouguerra-Aouichat, S., et al. Time-Restricted Feeding Improves Body Weight Gain, Lipid Profiles, and Atherogenic Indices in Cafeteria-Diet-Fed Rats: Role of Browning of Inguinal White Adipose Tissue. Nutrients 12(2020) 2185. https://doi.org/10.3390/nu12082185.

Dong, Y., Cheng, L., Zhao, Y. Resetting the circadian clock of Alzheimer's mice via GLP-1 injection combined with time-restricted feeding. Frontiers in physiology 13(2022) 911437. https://doi.org/10.3389/fphys.2022.911437.

Gudden, J., Arias Vasquez, A., Bloemendaal, M. The Effects of Intermittent Fasting on Brain and Cognitive Function. Nutrients 13(2021) 3166. https://doi.org/10.3390/nu13093166.

Gureev, A. P., Sadovnikova, I. S., Chernyshova, E. V., et al. Beta-Hydroxybutyrate Mitigates Sensorimotor and Cognitive Impairments in a Photothrombosis-Induced Ischemic Stroke in Mice. International journal of molecular sciences 25(2024) 5710. https://doi.org/10.3390/ijms25115710.

Valenzuela-Ahumada, L. A., Mercado-Gómez, O. F., Viveros-Contreras, R., et al. Fasting the mitochondria to prevent neurodegeneration: the role of ceramides. Frontiers in neuroscience 19(2025) 1602149. https://doi.org/10.3389/fnins.2025.1602149.

Martinez-Lopez, N., Mattar, P., Toledo, M., et al. mTORC2-NDRG1-CDC42 axis couples fasting to mitochondrial fission. Nature cell biology 25(2023) 989–1003. https://doi.org/10.1038/s41556-023-01163-3.

Zhang, X., Zhong, Y., Liu, L., et al. Fasting regulates mitochondrial function through lncRNA PRKCQ-AS1-mediated IGF2BPs in papillary thyroid carcinoma. Cell death & disease 14(2023) 827. https://doi.org/10.1038/s41419-023-06348-0.

Covarrubias, A. J., Perrone, R., Grozio, A., et al. NAD+ metabolism and its roles in cellular processes during ageing. Nature reviews. Molecular cell biology 22(2021) 119–141. https://doi.org/10.1038/s41580-020-00313-x.

Wu, L. E., Sinclair, D. A. SIRT2 controls the pentose phosphate switch. The EMBO journal 33(2014) 1287–1288. https://doi.org/10.15252/embj.201488713.

Zhuang, Y., Zhang, Y., Liu, C., et al. Interplay Between the Circadian Clock and Sirtuins. International journal of molecular sciences 25(2024) 11469. https://doi.org/10.3390/ijms252111469.

Naseer, A., Mir, S. S., Takacs-Vellai, K., et al. Sirtuins and Autophagy in Age-Associated Neurodegenerative Diseases: Lessons from the C. elegans Model. International journal of molecular sciences 22(2021) 12263. https://doi.org/10.3390/ijms222212263.

Zhang, Z., Zhang, L., Zhang, Y., et al. Inhibition of Sirtuin 2 enhances autophagy and restores neuronal function in aged hippocampal neurons. Brain research bulletin 230(2025) 111501. Advance online publication. https://doi.org/10.1016/j.brainresbull.2025.111501.

Rusek, M., Pluta, R., Ułamek-Kozioł, M., et al. Ketogenic Diet in Alzheimer's Disease. International journal of molecular sciences 20(2019) 3892. https://doi.org/10.3390/ijms20163892.

Van der Auwera, I., Wera, S., Van Leuven, F., et al. A ketogenic diet reduces amyloid beta 40 and 42 in a mouse model of Alzheimer's disease. Nutrition & metabolism 2(2005) 28. https://doi.org/10.1186/1743-7075-2-28.

Bohnen, J. L. B., Albin, R. L., Bohnen, N. I. Ketogenic interventions in mild cognitive impairment, Alzheimer's disease, and Parkinson's disease: A systematic review and critical appraisal. Frontiers in neurology 14(2023) 1123290. https://doi.org/10.3389/fneur.2023.1123290.

Oliveira, T. P. D., Morais, A. L. B., Dos Reis, P. L. B., et al. A Potential Role for the Ketogenic Diet in Alzheimer's Disease Treatment: Exploring Pre-Clinical and Clinical Evidence. Metabolites 14(2023) 25. https://doi.org/10.3390/metabo14010025.

Acharya, P., Acharya, C., Thongprayoon, C., et al. Incidence and Characteristics of Kidney Stones in Patients on Ketogenic Diet: A Systematic Review and Meta-Analysis. Diseases (Basel, Switzerland) 9(2021) 39. https://doi.org/10.3390/diseases9020039.

Zheng, Y., Sun, J., Luo, Z., et al. Emerging mechanisms of lipid peroxidation in regulated cell death and its physiological implications. Cell death & disease 15(2024) 859. https://doi.org/10.1038/s41419-024-07244-x.

de Oliveira, J., Engel, D. F., de Paula, G. C., et al. High Cholesterol Diet Exacerbates Blood-Brain Barrier Disruption in LDLr-/- Mice: Impact on Cognitive Function. Journal of Alzheimer's disease : JAD 78(2020) 97–115. https://doi.org/10.3233/JAD-200541.

Elias, A., Padinjakara, N., Lautenschlager, N. T. Effects of intermittent fasting on cognitive health and Alzheimer's disease. Nutrition reviews 81(2023) 1225–1233. https://doi.org/10.1093/nutrit/nuad021.

Manoogian, E. N. C., Chow, L. S., Taub, P. R., et al. Time-restricted Eating for the Prevention and Management of Metabolic Diseases. Endocrine reviews 43(2022) 405–436. https://doi.org/10.1210/endrev/bnab027.

Jiao, H., Kalsbeek, A., Yi, C. X. Microglia, circadian rhythm and lifestyle factors. Neuropharmacology 257(2024) 110029. https://doi.org/10.1016/j.neuropharm.2024.110029.

Currenti, W., Godos, J., Castellano, S., et al. Association between Time Restricted Feeding and Cognitive Status in Older Italian Adults. Nutrients 13(2021) 191. https://doi.org/10.3390/nu13010191.